Front. Optoelectron. 2013, 6(3): 243–250
DOI 10.1007/s12200-013-0333-y

RESEARCH ARTICLE

Nonlinear dynamics of 1550 nm VCSELs subject to polarization-preserved optical feedback and orthogonal optical injection

Bin WEI, Zhengmao WU, Tao DENG, Guangqiong XIA (✉)

School of Physical Science and Technology, Southwest University, Chongqing 400715, China

Abstract Based on spin-flip model (SFM), the nonlinear dynamics of 1550 nm vertical-cavity surface-emitting lasers (VCSELs) subject to polarization-preserved optical feedback (PPOF) and orthogonal optical injection (OOI) are theoretically investigated. The results show that two linear polarization (LP) modes can be simultaneously stimulated and polarization switching (PS) can be observed, which is different from the case that only y LP mode exists in a VCSEL with PPOF. Under the joint action of PPOF and OOI, the two LP modes will exhibit rich dynamical states, such as period one, period two, multi-period and chaos oscillation. Different evolution routes to chaos can be also observed. Moreover, frequency detuning Δf ($\Delta f = f_m - f_s$, where f_m and f_s are the center frequencies of free-running master VCSEL and slave VCSEL, respectively) has an obvious influence on the PS. With the increase of the positive frequency detuning PS points shift toward larger injection strengths; meanwhile, a suitable negative frequency detuning value makes the injection strength for PS be the lowest.

Keywords vertical-cavity surface-emitting lasers (VCSELs), nonlinear dynamics, orthogonal optical injection (OOI), polarization-preserved optical feedback (PPOF)

1 Introduction

Vertical-cavity surface-emitting lasers (VCSELs), as one of novel microchip lasers, have exhibited many prominent advantages over conventional edge-emitting semiconductor lasers (EESLs), such as single longitudinal-mode operation, low threshold current, excellent circular output beam with narrow divergence, low cost and easy large-scale integration into two-dimensional arrays, etc [1–5]. As a result, VCSELs are nowadays substituting traditional EESLs in many applications, such as fiber to home links, computer networks, optical interconnection and optical signal processing. Compared with free-running VCSELs, VCSELs subject to external perturbations, which include optical feedback, optical injection and optoelectronic feedback, display richer nonlinear dynamics [6–12]. So far, the nonlinear dynamics of VCSELs have been extensively investigated. Altés et al. experimentally and theoretically investigated the dynamic characteristics in VCSELs with orthogonal optical injection (OOI), and reported a stability map identifying boundaries between regions of stable locking, unlocking, bistability, and chaos [10]. Li et al. theoretically studied the static and dynamic characteristics of VCSELs with isotropic and polarization-selective optical feedback [11]. Paul et al. presented the polarization switching (PS) characteristics of VCSELs with orthogonal optical feedback [12]. Qader et al. investigated experimentally the effect of circularly polarized feedback on the polarization characteristics of VCSELs [13]. Above relevant studies are mainly concentrated on short-wavelength (< 1 μm) VCSELs.

The driving force for the development of long-wavelength (such as 1310 and 1550 nm) VCSELs, was mainly derived from the demands of increasing the communications distance to 10–20 km from the beginning, which is much longer than the 10–100 m of 850 nm short-wavelength VCSELs. However, as the telecoms market shifts from long-haul applications to local and access networks, long-wavelength VCSELs are newly attracting more and more attention [14]. With the spectacular increase in the traffic in local and access networks in recent years, the density of network systems have been required to be increased. As a result, the power consumption of the transceiver must be greatly decreased. Only

Received April 17, 2013; accepted April 26, 2013

E-mail: gqxia@swu.edu.cn

long-wavelength VCSELs, having one-tenth the consumption of EESLs, can meet this challenge. Moreover, with the improvement of the performances of long-wavelength VCSELs induced by the development of the production technology, long-wavelength VCSELs have been used in some new area such as sensor system, computer interconnects and other Si-related technologies due to their wavelength located at the low loss window of the silicon. With the expansion of the application area of long-wavelength VCSELs, the nonlinear dynamics of long-wavelength VCSELs, especially at the important telecom wavelength of 1550 nm, are paid more and more attention [15–21]. Chrostowski et al. demonstrated that injection locking greatly enhanced the resonance frequency of 1550 nm VCSELs [17]. The nonlinear dynamic characteristics of this kind of VCSELs subject to OOI were experimentally presented by Pérez et al. [18], and some behaviors different from those of short-wavelength VCSELs have been observed. Experimental study on the polarization switching and polarization bistability characteristics of 1550 nm VCSELs subject to polarized optical injection was performed by Hurtado et al. [19]. Al-Seyab et al. investigated theoretically and experimentally the dynamics of polarized optical injection in 1550 nm VCSELs, and how to determine the intrinsic parameter values of 1550 nm VCSELs have been given in detail [20]. The results show that some intrinsic parameters values for 1550 nm VCSELs are different from those of short-wavelength VCSELs, which inevitably results in the difference of dynamical behaviors between 1550 nm VCSELs and short-wavelength VCSELs. Compared with the systematic studies on 1550 nm VCSELs under single external perturbation, investigations on 1550 nm VCSELs under more than one external perturbation remain relatively scarce, though related studies on EESLs have shown that a nonlinear dynamical system with more than one external perturbation may possess some unique performances [22,23]. Moreover, considering that optical injection 1550 nm VCSELs are usually linked with other devices, and the influence of the residual optical feedback is difficult to be eliminated completely. Therefore, it is essential to study the nonlinear dynamic characteristics of 1550 nm VCSELs subject to optical feedback and optical injection. In this paper, based on spin-flip model (SFM), nonlinear dynamical characteristics of 1550 nm VCSELs subject to polarization-preserved optical feedback (PPOF) and OOI are numerically investigated.

2 System model and theory

Figure 1 is the schematic diagram of a 1550 nm VCSEL subject to PPOF and OOI. The output of a master-VCSEL (M-VCSEL) is first collimated by an aspheric lens (AL1), and then it is injected into a 1550 nm slave-VCSEL (S-VCSEL) via a neutral density filter (NDF1), a optical isolator (OI), a half wave plate (HWP) and two mirror (M2 and M3). Here, the angles between the direction of x linear polarization (LP) mode in M-VCSEL and the fast axis of the HWP are set as 45°. As a result, the x LP mode output from M-VCSEL is rotated into the direction of y LP mode of the S-VCSEL, while the y LP mode output from M-VCSEL is rotated into the direction of x LP mode of S-VCSEL before being injected into the S-VCSEL. OI is used for ensuring the unidirectional transmission of light. Two NDFs (NDF1 and NDF2) are used to adjust the injection and feedback strength, respectively.

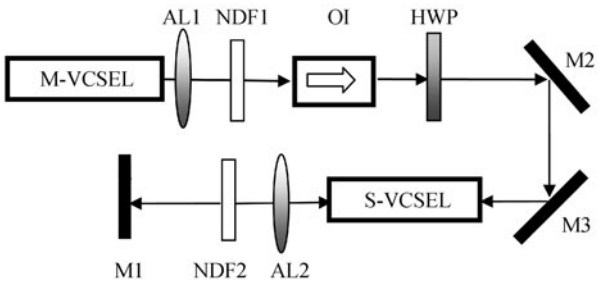

Fig. 1 Schematic diagram of 1550 nm VCSEL subject to PPOF and OOI. M-VCSEL: master-VCSEL. S-VCSEL: slave-VCSEL. HWP: half-wave plate. OI: optical isolator. M: mirror. NDF: neutral density filter. AL: aspheric lens

Based on the SFM [1], the rate equations for M-VCSEL and S-VCSEL can be described as

$$\frac{\mathrm{d}E^{\mathrm{m}}_{x,y}}{\mathrm{d}t} = k(1+\mathrm{i}\alpha)(N^{\mathrm{m}}E^{\mathrm{m}}_{x,y} - E^{\mathrm{m}}_{x,y} \pm \mathrm{i}n^{\mathrm{m}}E^{\mathrm{m}}_{y,x}) \mp (\gamma_{\mathrm{a}} + \mathrm{i}\gamma_{\mathrm{p}})E^{\mathrm{m}}_{x,y} + F^{\mathrm{m}}_{x,y}, \tag{1}$$

$$\frac{\mathrm{d}E^{\mathrm{s}}_{x,y}}{\mathrm{d}t} = k(1+\mathrm{i}\alpha)(N^{\mathrm{s}}E^{\mathrm{s}}_{x,y} - E^{\mathrm{s}}_{x,y} \pm \mathrm{i}n^{\mathrm{s}}E^{\mathrm{s}}_{y,x}) \mp (\gamma_{\mathrm{a}} + \mathrm{i}\gamma_{\mathrm{p}})E^{\mathrm{s}}_{x,y} + \eta E^{\mathrm{m}}_{y,x}(t-\tau_{\mathrm{s}})\mathrm{e}^{-\mathrm{i}2\pi f_{\mathrm{m}}\tau_{\mathrm{s}} + \mathrm{i}2\pi\Delta f t} + k_{\mathrm{f}}E^{\mathrm{s}}_{x,y}(t-\tau)\mathrm{e}^{-\mathrm{i}2\pi f_{\mathrm{s}}\tau} + F^{\mathrm{s}}_{x,y}, \tag{2}$$

$$\frac{\mathrm{d}N^{\mathrm{m,s}}}{\mathrm{d}t} = -\gamma_{\mathrm{e}}N^{\mathrm{m,s}}(1 + |E^{\mathrm{m,s}}_{x}|^2 + |E^{\mathrm{m,s}}_{y}|^2) + \gamma_{\mathrm{e}}\mu - \mathrm{i}\gamma_{\mathrm{e}}n^{\mathrm{m,s}}(E^{\mathrm{m,s}}_{y}E^{\mathrm{m,s}*}_{x} - E^{\mathrm{m,s}}_{x}E^{\mathrm{m,s}*}_{y}), \tag{3}$$

$$\frac{\mathrm{d}n^{\mathrm{m,s}}}{\mathrm{d}t} = -\gamma_{\mathrm{s}}n^{\mathrm{m,s}} - \gamma_{\mathrm{e}}n^{\mathrm{m,s}}(|E^{\mathrm{m,s}}_{x}|^2 + |E^{\mathrm{m,s}}_{y}|^2) - \mathrm{i}\gamma_{\mathrm{e}}N^{\mathrm{m,s}}(E^{\mathrm{m,s}}_{y}E^{\mathrm{m,s}*}_{x} - E^{\mathrm{m,s}}_{x}E^{\mathrm{m,s}*}_{y}), \tag{4}$$

where subscripts x and y stand for x and y LP modes, respectively, and superscripts m and s represent M-VCSEL and S-VCSEL, respectively. E is the slowly varied complex amplitude of the field, N is the total carrier inversion between the conduction and valence bands, n accounts for the difference between carrier inversions for the spin-up and spin-down radiation channels, k is the decay rate of field, α is the linewidth enhancement factor, γ_{e}

is the decay rate of total carrier population, γ_s is the spin-flip rate, γ_a and γ_p are the linear anisotropies representing dichroism and birefringence, respectively, k_f is the feedback strength, η is the injection strength from M-VCSEL to S-VCSEL. μ is the normalized injection current (μ takes the value 1 at threshold), τ is the feedback delay time, τ_s is the propagation delay time from M-VCSEL to S-VCSEL. Δf (= $f_m - f_s$, where f_m and f_s are the center frequencies of M-VCSEL and S-VCSEL, respectively) is the frequency detuning between the two VCSELs, and the spontaneous emission noises are modeled by the following Langevin sources:

$$F_x^{m,s} = \sqrt{\frac{\beta_{sp}^{m,s}}{2}} (\sqrt{N^{m,s} + n^{m,s}}\xi_1^{m,s} + \sqrt{N^{m,s} - n^{m,s}}\xi_2^{m,s}), \quad (5a)$$

$$F_y^{m,s} = -i\sqrt{\frac{\beta_{sp}^{m,s}}{2}} (\sqrt{N^{m,s} + n^{m,s}}\xi_1^{m,s} - \sqrt{N^{m,s} - n^{m,s}}\xi_2^{m,s}), \quad (5b)$$

where ξ_1 and ξ_2 indicate independent Gaussian white noise with zero mean and unitary variance, and β_{sp} is the spontaneous emission rate.

3 Results and discussion

Equations (1)–(4) can be numerically solved by adopting fourth-order Runge-Kutta algorithm. During calculations, the internal parameters for the two VCSELs are assumed to be identical, and the used parameters are described as follows [20,21]: $\alpha = 2.2$, $k = 125\ ns^{-1}$, $\beta_{sp} = 10^{-5}\ ns^{-1}$, $\gamma_e = 0.67\ ns^{-1}$, $\gamma_s = 1000\ ns^{-1}$, $\gamma_a = 1\ ns^{-1}$, $\gamma_p = 192\ ns^{-1}$. Meanwhile, both the delay feedback time τ and the injection time τ_s are set to be 2 ns and the oscillation frequency f_s of S-VCSEL is fixed at 194.33 THz (corresponding central wavelength is about 1543 nm).

Figure 2 gives the polarization-resolved *P-I* curve for a free-running 1550 nm VCSEL. During numerical simulations, the intensities are averaged over a time window of 200 ns. As shown in Fig. 2, when the normalized injection current $\mu > 1$, only *y* LP mode (solid line) oscillates and *x* LP mode is always suppressed, and then no PS emerges over the given bias current range. This can be explained as that, comparing with short-wavelength VCSELs, 1550 nm VCSELs have a larger anisotropy coefficient γ_a and frequency splitting between two orthogonal polarization modes [21].

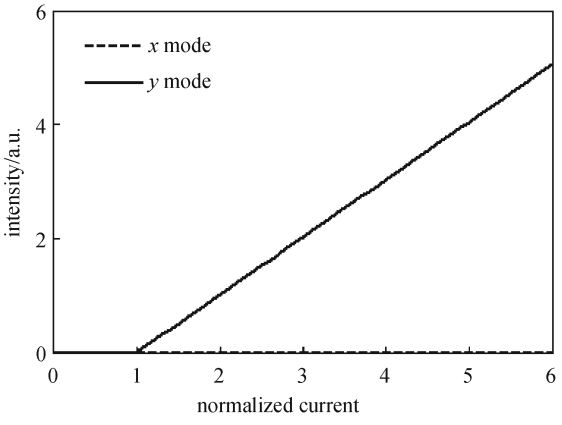

Fig. 2 Polarization-resolved *P-I* curve for a free-running VCSEL. Dotted line is for *x* LP mode and solid line is for *y* LP mode

3.1 Dynamics of 1550 nm VCSEL subject to PPOF

First, we investigate the dynamics of a 1550 nm VCSEL with PPOF. Figure 3 displays the bifurcation diagrams of the extrema of peak series with feedback strength for μ = 1.5. As shown in Fig. 3(b), with the increase of the feedback strength, a variety of nonlinear dynamical behaviors including period-one (P1), multi-periodic (MP) and chaotic oscillation (CO) have been observed for *y* LP mode. When the feedback strength $k_f < 0.6\ ns^{-1}$, *y* LP mode operates at the steady-state. With the increase of the feedback strength from 0.6 to 1.8 ns^{-1}, *y* LP mode goes through P1, MP route to CO. Further increasing the

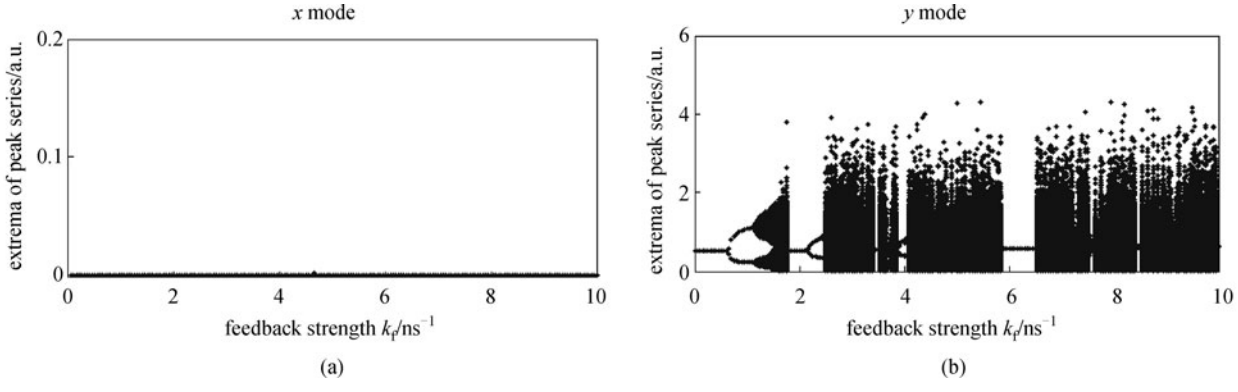

Fig. 3 Bifurcation diagrams of extrema of peak series versus feedback strength k_f for μ = 1.5. (a) *x* mode; (b) *y* mode

feedback strength to 2.2 ns^{-1}, y LP mode operates at the steady-state again. When the feedback strength increases from 2.2 to 3.4 ns^{-1}, y LP mode experiences P1 route to chaos. With further increasing the feedback strength, similar evolution route to chaos can be observed. It should be pointed out that, although the dynamical states and routes to chaos are rather rich, only y LP mode acts as a dominant role while x LP mode is suppressed within the given feedback strength range.

3.2 Influence of OOI on dynamical characteristics of VCSELs with PPOF

After introducing an OOI from M-VCSEL, the dynamics of S-VCSEL become richer under the joint action of the optical injection and optical feedback.

3.2.1 Influence of injection strength

Figure 4 shows the bifurcation diagrams of the peak series with feedback strength k_f under different injection strengths for $\mu = 1.5$ and $\Delta f = 0$ GHz. From this diagram, it can be seen that both of two LP modes are simultaneously stimulated and exhibit rich dynamics. Different from above case for only PPOF, some new states such as period-two (P2) and period-four (P4) oscillation have been observed for $\eta = 300$ ns^{-1} (as shown in Figs. 4 (a3) and 4(b3)). As a result, some new routes to chaos can be observed.

Figure 5 shows different routes to chaos for x LP mode and y LP mode, where the time series, the power spectra, and the phased portraits of different states are plotted, respectively. The injection strength is fixed at 300 ns^{-1} while the feedback strengths take different values of k_f = 0.8, 1.2, 1.3 and 1.4 ns^{-1} for corresponding states. Obviously, for $k_f = 0.8$ ns^{-1}, the states of both x and y LP modes are P1 (see Figs. 5(a1)–5(a2)) with a fundamental frequency of 1.62 GHz. For $k_f = 1.2$ ns^{-1} (see Figs. 5(b1)–5 (b2)), both of x and y LP modes operate at P2 state, where the sub-harmonic frequencies can be seen in the power spectra while two dots emerge in the phase portraits. For k_f = 1.3 ns^{-1}, as shown in Figs. 5(c1) – 5(c2), the state of x LP mode is period-four (P4) but the state of y LP mode is multi-period (MP) state. For $k_f = 1.4$ ns^{-1} (see Figs. 5(d1)–5(d2)), the outputs of both x and y LP modes vary chaotically, and the corresponding power spectrum are continuous meanwhile the phase portraits show highly scattered distribution in a large area. Under this case, both x and y LP modes operate at the chaotic state.

Previous investigations have demonstrated that OOI

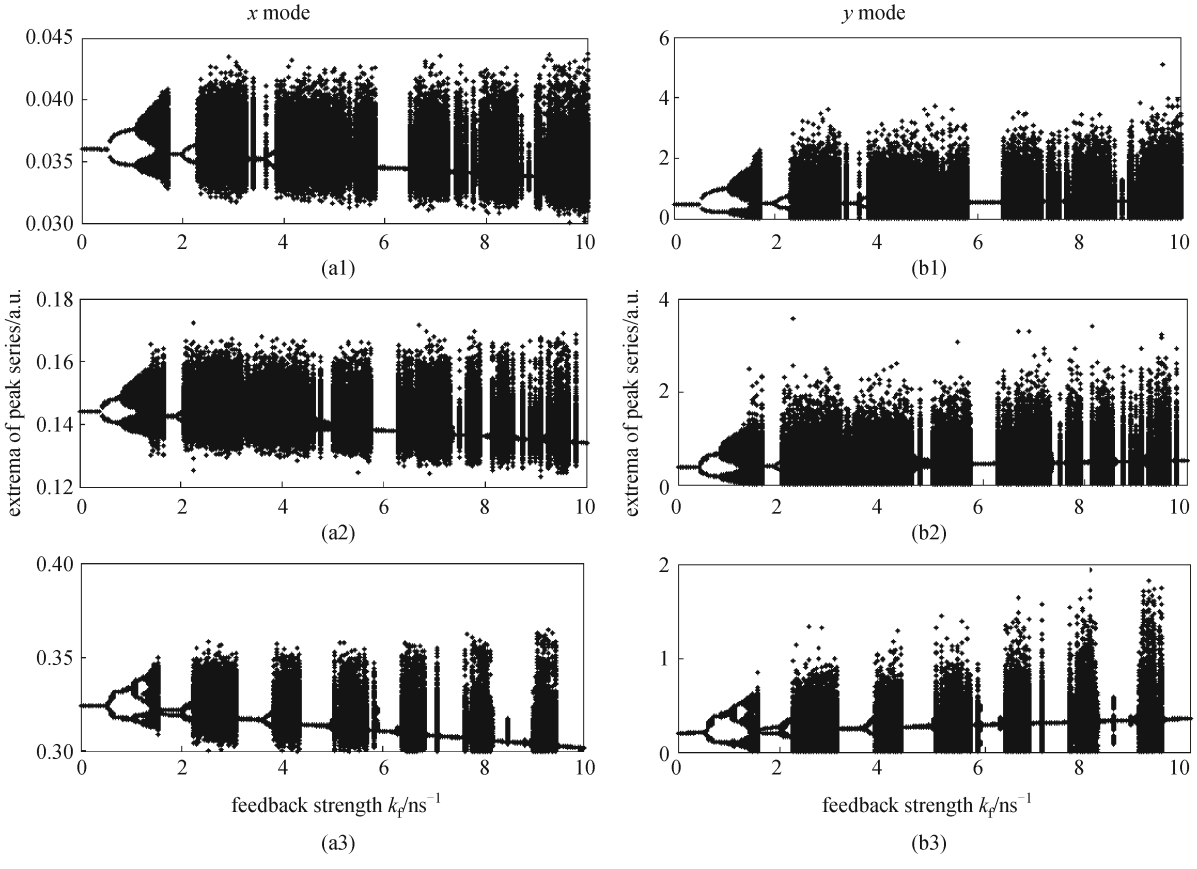

Fig. 4 Bifurcation diagrams of extrema of peak series versus different feedback strength k_f for $\mu = 1.5$ and $\Delta f = 0$ GHz with $\eta = 100$ ns^{-1} (a1, b1), 200 ns^{-1} (a2, b2), and 300 ns^{-1} (a3, b3)

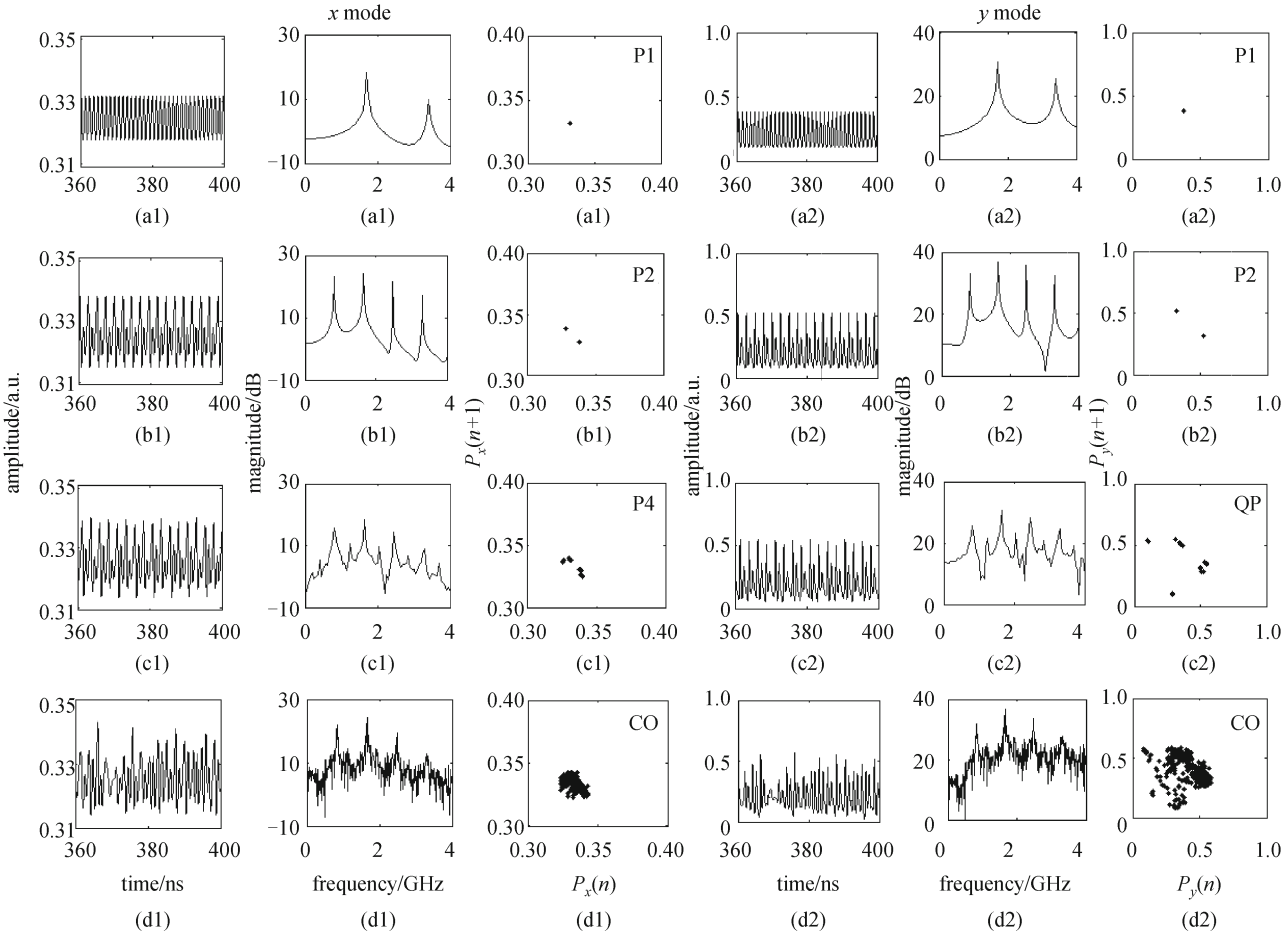

Fig. 5 Time series, power spectra, and phase portraits of different states with $\mu = 1.5$, $\eta = 300\ \text{ns}^{-1}$ and $\Delta f = 0$ GHz, where (a)–(d) correspond to $k_f = 0.8$, 1.2, 1.3 and $1.4\ \text{ns}^{-1}$, respectively

may result in PS [6]. Obviously, the introduction of PPOF will inevitably affect the characteristic of PS induced by OOI. Figure 6 gives the curves of normalized mean output power against injection strength under different feedback strengths for $\mu = 1.5$ and $\Delta f = 0$ GHz. It can be seen that, with the increase of injection strength, the mean power of x LP mode gradually increases while mean power of y LP mode exhibits a decreasing tendency, and then PS will occur once the injection strength reaches a certain value. With the increase of the feedback strength of PPOF, the value of injection strength needed for PS will increase. The reason is that PPOF have enlarged the intensity difference between two LP modes compared with the case that no PPOF is introduced. As a result, a larger value of injection strength is required to realize PS for a 1550 nm VCSEL subject to PPOF.

3.2.2 Influence of frequency detuning

To reveal the influences of the frequency detuning on dynamic characteristics of 1550 nm VCSEL with PPOF and OOI, Fig. 7 simulates the bifurcation diagrams of the extrema of the peak series with feedback strength k_f under different frequency detuning Δf, where the injection strength η is fixed at $100\ \text{ns}^{-1}$. From these diagrams, it can be seen that there exist a similar evolution process but the ranges of different states is varied with Δf.

Furthermore, we investigate the impact of frequency detuning on PS. Figure 8 displays normalized mean output powers of two modes versus injection strength under different frequency detuning. From these diagrams, it can be seen that frequency detuning has an obvious effect on the location of PS point. For positive frequency detuning, the PS point shifts toward larger injection strength with the increase of the detuning frequency. For negative frequency detuning, with the increase of absolute value of Δf, the PS point shifts toward lower inject strength first, after reach the lowest injection strength required for PS, and then shift toward larger inject strength.

4 Conclusions

Based on the SFM, the nonlinear dynamical characteristics

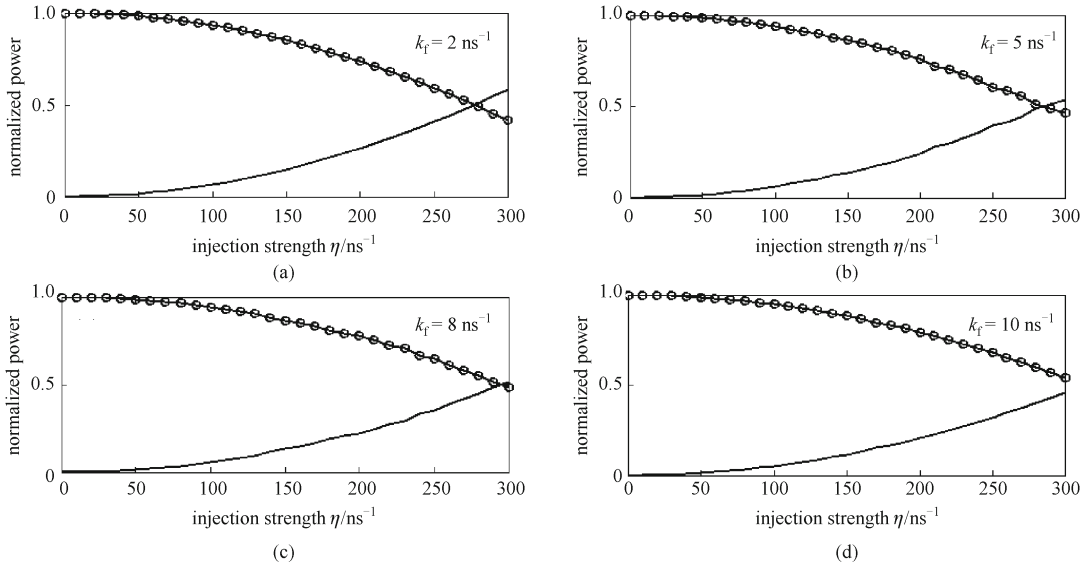

Fig. 6 Normalized mean output powers versus injection strength for $\mu = 1.5$ and $\Delta f = 0$ GHz, where solid line corresponds to x LP mode and solid line with circles corresponds to y LP mode, and (a)–(d) correspond to feedback strength k_f = 2, 5, 8, 10 ns^{-1}, respectively

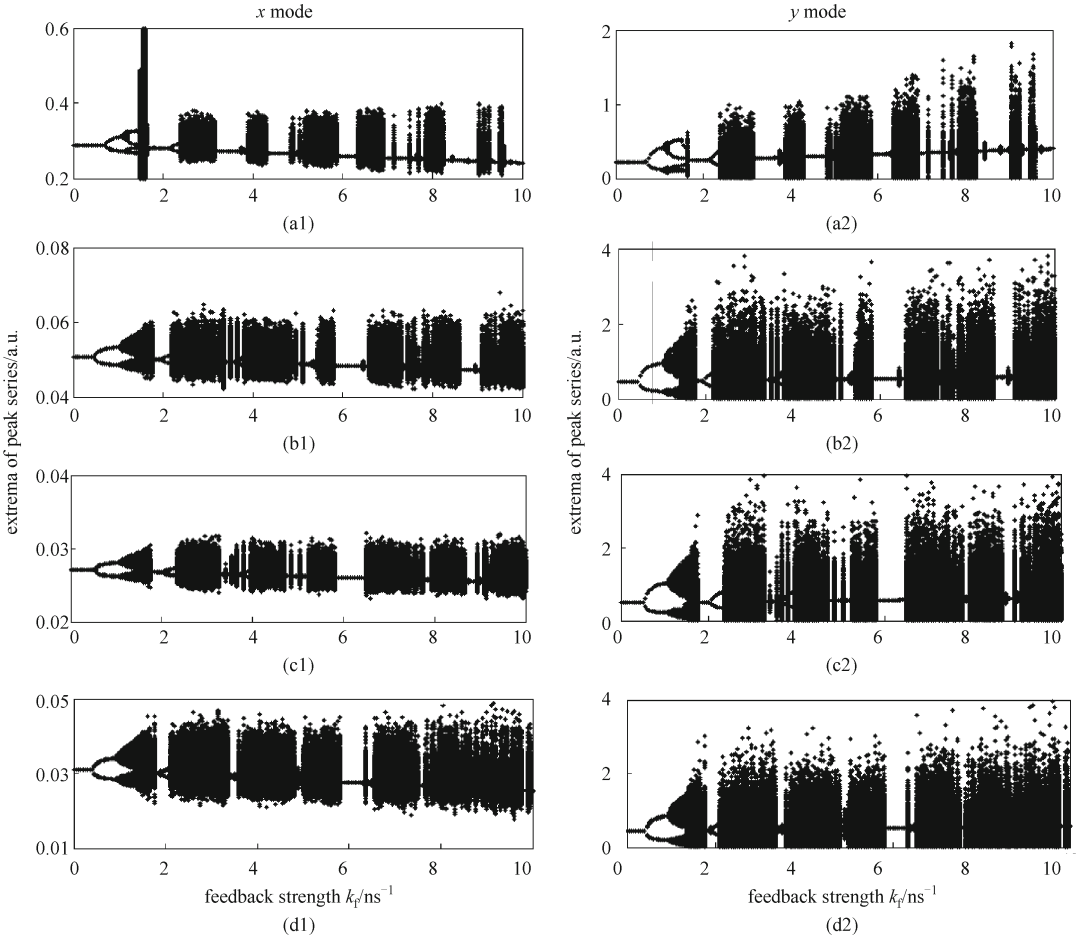

Fig. 7 Bifurcation diagrams of extrema of peak series versus feedback strength k_f for $\mu = 1.5$ and $\eta = 100$ ns^{-1}, where (a)–(d) correspond to frequency detuning Δf = –40, –10, 10, 40 GHz, respectively

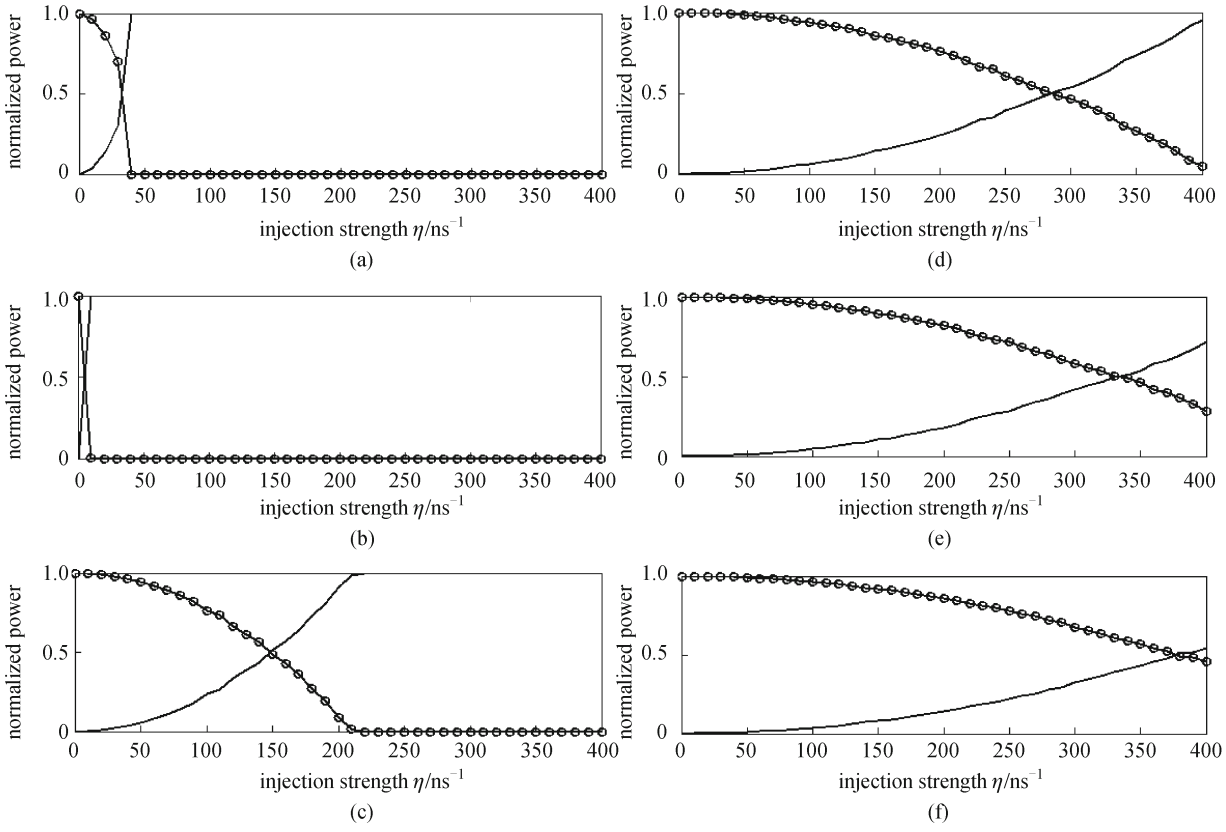

Fig. 8 Normalized mean powers for two LP modes versus injection strength for μ = 1.5 and k_f = 5 ns^{-1} with different frequency detuning, where solid line corresponds to x LP mode and solid line with circles corresponds to y LP mode, and (a)–(f) correspond to frequency detuning Δf = –70, –60, –30, 0, 10, 20 GHz, respectively

of a 1550 nm VCSEL subject to OOI and PPOF is theoretically investigated. The simulated results show that, after introducing OOI to a 1550 nm VCSEL with PPOF, two LP modes of S-VCSEL can simultaneously oscillate and exhibit rich and similar dynamic behaviors. Many different evolution routes to chaos such as period-one route to chaos, period-doubling route to chaos, and P1, P2, multi-periodic routes to chaos have been found in such a proposed system. Additionally, the PS phenomena induced by OOI have been investigated. PPOF makes the required injection strength for PS increase, and negative frequency detuning is helpful to obtain lower injection strength for realizing PS. It is hoped that this work is helpful to control the dynamic state and PS performances of 1550 nm VCSELs.

Acknowledgements This work was supported by the National Natural Science Foundation of China (Grant Nos. 60978003, 61078003, 61178011 and 61275116) and the Natural Science Foundation of Chongqing City (No. 2012jjB40011).

References

1. Miguel M S, Feng Q, Moloney J V. Light-polarization dynamics in surface-emitting semiconductor lasers. Physical Review A, 1995, 52 (2): 1728–1739
2. Chang-Hasnain C J. Tunable VCSEL. IEEE Journal on Selected Topics in Quantum Electronics, 2000, 6(6): 978–987
3. Liu J, Wu Z M, Xia G Q. Dual-channel chaos communication in unidirectional coupled VCSELs with polarization-rotated optical feedback and polarization-rotated optical injection. Optics Express, 2009, 17(15): 12619–12626
4. Debernardi P, Ostermann J M, Feneberg M, Jalics C, Michalzik R. Reliable polarization control of VCSELs througth monolithically integrated surface gratings: a comparative theoretical and experiment study. IEEE Journal on Selected Topics in Quantum Electronics, 2005, 11(1): 107–116
5. Arteaga M A, Unold H J, Ostermann J M, Michalzik R, Thienpont H, Panajotov K. Investigation of polarization properties of VCSELs subject to optical feedback from an extremely short external cavity—part I: theoretical analysis. IEEE Journal of Quantum Electronics, 2006, 42(2): 89–101
6. Gatare I, Buesa J, Thienpont H, Panajotov K, Sciamanna M. Polarization switching bistability and dynamics in vertical-cavity surface-emitting semiconductor laser under orthogonal optical injection. Optical and Quantum Electronics, 2006, 38(4–6): 429–443
7. Wang X F, Xia G Q, Wu Z M. Theoretical investigations on the

polarization performances of current-modulated VCSELs subject to weak optical feedback. Journal of the Optical Society of America B, Optical Physics, 2009, 26(1): 160–168

8. Hong Y, Spencer P S, Rees P, Shore K A. Optical injection dynamics of two-mode vertical-cavity surface-emitting semiconductor lasers. IEEE Journal of Quantum Electronics, 2002, 38(3): 274–278
9. Xiao P, Wu Z M, Wu J G, Jiang L, Deng T, Tang X, Fan L, Xia G Q. Time-delay signature concealment of chaotic output in a vertical-cavity surface-emitting laser with double variable-polarization optical feedback. Optics Communications, 2013, 286(1): 339–343
10. Altés B J, Gatare I, Panajotov K, Thienpont H, Sciamanna M. Mapping of the dynamics induced by orthogonal optical injection in VCSELs. IEEE Journal of Quantum Electronics, 2006, 42(2): 198–207
11. Li X F, Pan W, Luo B, Ma D, Deng G. Static and dynamic characteristics of VCSELs with polarization-selective optical feedback. Optoelectronics, IEE Proceedings-, 2006, 153(2): 67–74
12. Paul J, Masoller C, Hong Y H, Spencer P S, Shore K A. Impact of orthogonal optical feedback on the polarization switching of vertical-cavity surface-emitting lasers. Journal of the Optical Society of America B, Optical Physics, 2007, 24(8): 1987–1994
13. Qader A A, Hong Y, Shore K A. Circularly polarized optical feedback effects on the polarization of VCSEL emission. IEEE Photonics Technology Letters, 2012, 24(14): 1200–1202
14. Kapon E, Sirbu A. Long-wavelength VCSELs: power-efficient answer. Nature Photonics, 2009, 3(1): 27–29
15. Hurtado A, Quirce A, Valle A, Pesquera L, Adams M J. Nonlinear dynamics induced by parallel and orthogonal optical injection in 1550 nm vertical-cavity surface-emitting lasers (VCSELs). Optics Express, 2010, 18(9): 9423–9428
16. Zheng A J, Wu Z M, Deng T, Li X J, Xia G Q. Investigation on nonlinear dynamics of 1550 nm vertical-cavity surface-emitting lasers with polarization-preserved optical feedback. Acta Physica Sinica, 2012, 61(23): 234203
17. Chrostowski L, Faraji B, Hofmann W, Amann M C, Wieczorek S, Chow W W. 40 GHz bandwidth and 64 GHz resonance frequency in injection-locked 1.55 μm VCSELs. IEEE Journal on Selected Topics in Quantum Electronics, 2007, 13(5): 1200–1208
18. Pérez P, Quirce A, Pesquera L, Valle A. Polarization-resolved nonlinear dynamics induced by orthogonal optical injection in long-wavelength VCSELs. IEEE Journal on Selected Topics in Quantum Electronics, 2011, 17(5): 1228–1235
19. Hurtado A, Henning I D, Adams M J. Wavelength polarization switching and bisability in a 1550 nm VCSEL subject to polarized optical injection. IEEE Photonics Technology Letters, 2009, 21(15): 1084–1086
20. Al-Seyab R, Schires K, Khan N A, Hurtado A, Henning I D, Adams M J. Dynamics of polarized optical injection in 1550-nm VCSELs: theory and experiments. IEEE Journal on Selected Topics in Quantum Electronics, 2011, 17(5): 1242–1249
21. Torre M, Hurtado A, Quirce A, Valle A, Pesquera L, Adams M. Polarization switching in long-wavelength VCSELs subject to orthogonal optical injection. IEEE Journal of Quantum Electronics, 2011, 47(1): 92–99
22. Wu J G, Xia G Q, Wu Z M. Suppression of time delay signatures of chaotic output in a semiconductor laser with double optical feedback. Optics Express, 2009, 17(22): 20124–20133
23. Wang A B, Wang Y C, He H C. Enhancing the bandwidth of the optical chaotic signal generated by a semiconductor laser with optical feedback. IEEE Photonics Technology Letters, 2008, 20(19): 1633–1635